JOURNAL OF PHYSICAL CHEMISTRY, 2025, Vol. 99, No. 1, c. 90–98

PHYSICAL CHEMISTRY OF SOLUTIONS

SYNTHESIZING METAL-ORGANIC UIO-66 FRAMEWORK IN MICROWAVE FIELDS BASED ON POLYETHYLENE TEREPHTHALATE WASTE FOR ADSORPTIVE REMOVAL OF TARTRAZINE FOOD DYE FROM AQUEOUS SOLUTIONS

V. V. Vergun[a], *, M. D. Vedenyapina[a], S. A. Kulaishin[a], V. V. Chernyshev[b,c], O. P. Tkachenko[a], V. D. Nissenbaum[a], and V. I. Isaeva[a]

[a]*Zelinsky Institute of Organic Chemistry of Russian Academy of Sciences, Moscow, Russia*

[b]*Frumkin Institute of Physical Chemistry and Electrochemistry of the Russian Academy of Sciences, Moscow, Russia*

[c]*Lomonosov Moscow State University, Moscow, Russia*

**e-mail: polubrat@mail.ru*

Received April 12, 2024
Revised April 12, 2024
Accepted April 26, 2024

Abstract. The sample of metal-organic UiO-66 framework ($Zr_6O_4(OH)_4$bdc, bdc = benzene-1,4-dicarboxylate/terephthalate), which is a promising adsorbent of persistent organic pollutants from aqueous medium, is obtained by the original method in the medium of unconventional "green" solvent, triethylene glycol (TEG), under conditions of microwave activation of reaction mass at atmospheric pressure according to one-step approach. PET-UiO-66 material is synthesized using polymer waste, viz. recycled polyethylene terephthalate (PET), as a source of organic linker (terephthalic or benzene-1,4-dicarboxylic acid, H_2bdc) for framework formation. Its adsorption activity is first studied in the adsorption removal of tartrazine food dye (E-102) from aqueous solutions. It is found that the kinetics of the adsorption process obeys the pseudo-second-order model, and its thermodynamics corresponds to the Langmuir model.

Keywords: *metal-organic frameworks (MOF), polyethylene terephthalate (PET), UiO-66, adsorption from aqueous medium, kinetics*

DOI: 10.31857/S00444537250109e4

Nowadays, accumulation of various wastes, both industrial and by-products of everyday activities poses a serious threat to the environment and, thus, to human health and life [1]. They are present almost everywhere, in urban disposal sites, in surface and ground water, as well as in forests. On the other hand, there is an increasing need to replace non-renewable sources of raw materials for obtaining important products and intermediates of the chemical industry with renewable analogs. To solve these problems, an integrated approach is needed that includes waste treatment and recycling and, in the case of hazardous substances and materials, decomposition or elimination to avoid secondary contamination [2, 3].

Accumulation of polymer wastes poses a special threat since their slow aging and degradation in natural conditions, primarily under the influence of UV radiation, release a variety of toxic substances. As a rule, polymer waste is resistant to biodegradation, unlike organic waste. Due to their gradual photodegradation under the influence of sunlight, small fragments (microplastics) are formed, which is lethal for living organisms (fish, mammals) that can consume it with food [4, 5]. The most common polymer wastes are polyester polymers such as PET, polybutylene terephthalate (PBT), and polylactide (PLA). In particular, PET is extremely resistant to degradation in natural conditions.

A promising approach to solving the problem of removing polymer waste products from the environment is their conversion into value-added products. Thus, the technology of their conversion by pyrolysis and thermal treatment (including the use of catalysts) is developed to produce fuel and valuable chemical intermediates, such as acids, aldehydes, and ketones [6, 7]. This strategy corresponds to the principles of the closed-cycle economy, which is a more progressive alternative to the traditional linear economy.

The following stages of PET waste recycling are known, viz. primary recycling, secondary recycling

(mechanical or physical recycling), and tertiary recycling (chemical recycling) [8], with chemical depolymerization being recognized as the most promising approach. Currently, ways to further improve the environmental friendliness of PET recycling processes are being studied. Thus, a method of its catalytic depolymerization (glycolysis) with the formation of bis(2-hydroxyethyl)terephthalate in the presence of metal azolate framework MAF-6 in the diethylene glycol medium is developed [9].

In addition to polymer waste, a serious source of environmental pollution lies in accumulation of persistent organic pollutants (POP) in wastewater, which are also virtually impossible to remove by chemical, photolytic, and biological methods. As a consequence, POP may be present in tap water in trace amounts after filtration systems. These substances include pharmaceuticals, organic dyes, and herbicides. Adsorption on nanoporous materials is the most effective method for POP removal from aqueous media. A relatively new class of porous coordination polymers — metal-organic frameworks (MOF) — holds especially great potential in this respect. By nature, they are coordination polymers, their three-dimensional structure formed by ions or small clusters of metals connected by polydentate organic ligands (linkers) [10]. Due to their unique physicochemical properties, MOF can be used in gas-phase [11] and liquid-phase adsorption [12], (photo)catalysis [13], electrochemistry [14], and biomedicine [15].

To date, many MOF materials have been studied in the POP adsorptive removal processes of from water [16]. The most promising adsorbents of this kind include UiO-66 ($Zr_6O_4(OH)_4$bdc, bdc = benzene-1,4-dicarboxylate/terephthalate) [17] and its analog NH_2-UiO-66 with aminoterephthalate (2-aminobenzene-1,4-dicarboxylate (abdc)) linkers [18]. These carriers are characterized by increased chemical stability at pH values of the medium varying in a wide range. The (NH_2)-UiO-66 adsorbents have demonstrated efficiency in the removal processes for various POP [19, 20] as well as inorganic particles [21] from water.

Terephthalic acid is a source of organic linker for building the structure of numerous MOF materials [22], including the UiO-66 framework. In terms of practical applications of adsorbents of this kind, an important challenge is to find cost-effective renewable sources of the respective linker. A promising approach to solve it to depolymerize PET waste with the release of terephthalate linker [23]. This method can be realized in one or two stages. In the first case, depolymerization with the terephthalic acid formed occurs at a separate stage followed by obtaining MOF material. In the second case, the MOF sample is synthesized directly from the polymer waste. For instance, a one-step method was used to prepare a series of nanoporous materials MIL-47, MIL-53(Cr), MIL-53(Al), MIL-53(Ga), and MIL-101(Cr) [24]. In this case, PET waste is introduced into the solvothermal process along with the salt of the respective metal in a proper solvent, and PET depolymerization occurs simultaneously with the formation of the MOF sample.

In publications, there are examples of UiO-66 material preparation using PET waste as a source of terephthalate linker by both two-stage [25, 26] and one-stage methods. Thus, the UiO-66 sample obtained from PET waste according to the two-stage method was used for extraction and preconcentration of the steroid hormones such as progesterone, hydrocortisone, 17β-estradiol, and estrone in river water samples by high-performance liquid chromatography [27].

The UiO-66 material with a bdc-linker based on secondary PET was prepared by a one-stage method under solvothermal conditions under microwave heating (200°C, 500 W, 30 min) in the presence of hydrochloric acid as a depolymerization catalyst. This sample showed efficiency in adsorption of carbon dioxide [28].

In this work, the PET-UiO-66 material was synthesized by an original methodology according to a one-stage approach. The reaction was carried out under microwave activation of the reaction mass at atmospheric pressure (260°C 200 W, 30 min) in the environmentally friendly solvent triethylene glycol (TEG). The terephthalate formed by thermal depolymerization of PET, which is a waste of uncolored plastic bottles from soft drinks, was used to form the framework. The process was implemented without using HCl or other additional agents that promote depolymerization. The PET-UiO-66 sample was studied by powder X-ray diffraction analysis (pXRD), infrared spectroscopy (DRIFTS), electron microscopy (TEM, SEM) and thermogravimetric analysis (TGA).

The adsorption activity of the PET-UiO-66 material was first studied against tartrazine (a typical POP), a dye used for coloring food products and drug capsule shells, and toxic at high concentrations (Fig. 1). Note that publications only describe single examples of adsorption of tartrazine from aqueous solutions on the UiO-66 material and its modified analogs obtained using commercially available terephthalic acid [29, 30].

EXPERIMENTAL PART

We used commercially available reagents (c. p.) without additional purification. We used fragments of plastic containers for soft drinks (~2 × 2 mm) as secondary PET without additional treatment.

Synthesis of PET-UiO-66. The starting reagents $ZrOCl_2 \times 8H_2O$ (5.0 mmol, 1.62 g), PET (0.96 g), and TEG (20 mL) were loaded into a glass reactor. The synthesis was carried out under microwave activation of the reaction mixture (200 W, 30 min) in the chamber of a modified Panasonic NN-GD366M microwave oven. During the process, the temperature of the reaction mixture increased and reached 260°C after 20 min from the start. After the reaction mixture was cooled, the PET-UiO-66 sample was separated by centrifugation, washed with distilled water (2 × 20 mL), methanol (2 × 20 mL), dried under reduced pressure and evacuated (150°C, 10^{-3} mmHg, 8 h). The yield of the target product was 81.3%.

Synthesis of the classic-UiO-66 reference sample. The sample classic-UiO-66 was prepared according to the known technique [18].

Physicochemical characterization of the PET-UiO-66 material. The microstructure of the synthesized samples was studied using transmission (STEM) and scanning (SEM) electron microscopy. Analytical measurements was optimizzed within the framework of the previously described approach [31]. Prior to imaging, the sample was placed onto the surface of a 25 mm diameter aluminum stage, fixed using a conductive carbon tape, and sputtered with a 10 nm thick Au conductive layer using the magnetron sputtering method described previously [32]. The microstructure of the sample was studied by scanning field emission electron microscopy (STEM) on a Hitachi Regulus 8230 electron microscope. Images were captured in the mode of backscattered electron registration (composite contrast) at an accelerating voltage of 10 kV. The sample was studied by X-ray spectral microanalysis (EDS-SEM) using a Bruker Quantax 400 microanalysis system with an XFlash 6|60 detector at an accelerating voltage of 20 kV.

X-ray measurements were performed at room temperature on an EMPYREAN diffractometer (Panalytical, The Netherlands) (CuK_α radiation, nickel filter, X′Celerator linear detector, Bragg-Brentano geometry). Fourier-transform infrared spectra (DRIFTS) were recorded at room temperature using a Nicolet 460 Protege spectrometer (USA) equipped with an attachment for diffuse scattering measurements. The samples were placed in an ampoule equipped with a KBr window. The samples were treated in vacuum at 150°C (2 h) before recording FTIR spectra. To obtain a satisfactory signal-to-noise ratio, 500 scans were recorded for each spectrum. The spectra were measured from 400 to 6000 cm^{-1} with a resolution of 4 cm^{-1}. The intensity of absorption bands (AB) in the spectra were estimated in Kubelka-Munk units.

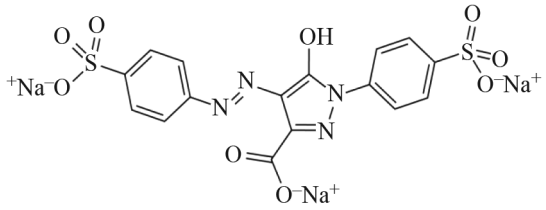

Fig. 1. Structural formula of tartrazine.

Adsorption of tartrazine from aqueous solutions with an initial concentration of 150–25 mg/L was carried out under constant stirring on a magnetic stirrer (150 rpm) at room temperature. While achieving adsorption equilibrium, its concentration in the solution was determined spectrophotometrically by absorbance at a wavelength of 440 nm on Hitachi U-1900 (Japan). TGA measurements were carried out in air up to 750°C at a rate of 10°C/min on a Derivatograph-C unit (MOM).

DISCUSSION OF RESULTS

Synthesis of the PET-UiO-66 sample. The PET-UiO-66 sample was prepared by a one-stage method under microwave activation of the reaction mass at atmospheric pressure according to the original methodology. The use of a non-conventional TEG solvent with a high boiling point (285°C) allows the process to be carried out at atmospheric pressure in the absence of acids and other aggressive agents contributing to PET depolymerization. At the same time, the reaction time (30 min) is significantly reduced as compared to the synthesis of the classic-UiO-66 sample according to the published method (solvothermal conditions, 24 h) [17]. The concentration of Zr^{4+} ions (0.25 M) during synthesis of the PET-UiO-66 material (Zr^{4+} : PET in the 1 : 1 ratio) significantly exceeds the concentration of zirconium (IV) salt during the preparation of the classic-UiO-66 sample (0.001 M) [17], as well as the concentration during the synthesis of the published UiO-66 analog based on PET waste (0.1 M) [28]. Note that carrying out the reaction at high concentrations of reagents reduces the solvent (TEG) consumption, thereby increasing the process performance (in terms of g/(l·min)). These conditions, along with the use of PET waste as a source of the bdc-linker and energy-saving microwave synthesis, contribute to practical application of the PET-UiO-66 material.

Studying physicochemical characteristics of the PET-UiO-66 sample. The X-ray diffractogram of the PET-UiO-66 material (Fig. 2) shows three very broad peaks, which indicates extremely small sizes of the coherent scattering regions, not exceeding several nanometers. At the same time, the location of these

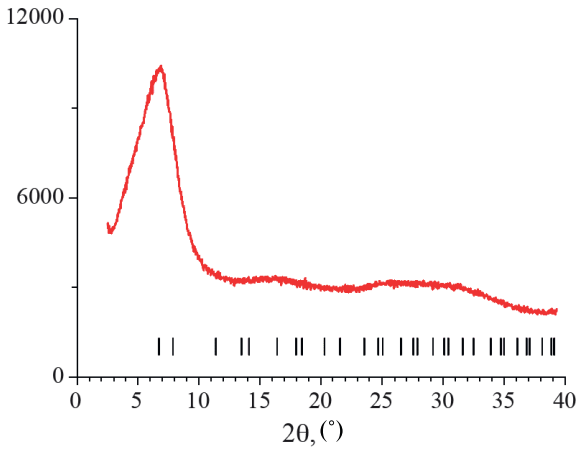

Fig. 2. Diffractogram of the PET-UiO-66 material. Vertical segments show the calculated positions of reflections for the classical UiO-66 structure with the cubic cell parameter a = 20.75 A and the *Fm-3m* spatial symmetry group.

peaks is quite consistent with the positions and relative heights of the peaks of the classical UiO-66 structure, taking into account their broadening due to small crystallite sizes.

Figure 3 shows SEM (left) and STEM (right) micrographs of the PET-UiO-66 material. The material involved consists of irregularly shaped particles of size 30–100 nm organized in dense agglomerates; a developed system of macropores can also be observed. The sample is homogeneous and contains no visible inclusions of the original PET. Figure 4 shows the elemental mapping of the PET-UiO-66 material (on the carbon substrate). The uniform distribution of the elements included in the material is observed, which indicates its homogeneity.

Spectral characteristics of PET-UiO-66. The functional groups on the surface of the PET-UiO-66 sample, which significantly affect its adsorption behavior, were studied by the DRIFTS method. In order to identify the features of its chemical composition, its spectral characteristics were compared with the classic-UiO-66 reference sample.

Figure 5 shows the overview IR spectra of the classic-UiO-66 and PET-UiO-66 samples after thermal vacuum treatment (150°C).

The bands in the region 3700–3200 cm^{-1} are characteristic of the interaction of the surface of classic-UiO-66 and PET-UiO-66 with adsorbate molecules, primarily water. Vacuum treatment at 150°C leads to partial removal of adsorbates.

The intense distinct band in the spectrum of the classic-UiO-66 reference sample at 3673 cm^{-1} is characteristic of O–H groups in the μ_3-OH bridge fragment [33, 34]. In the PET-UiO-66 spectrum, the same groups appear as a small intense band at 3433 cm^{-1} [33–38]. A broad band in the spectra of both samples in the region 3600–3200 cm^{-1} indicates valence vibrations of O-H groups involved in hydrogen bonding [33-38].

The bands at 3072, 2993, 2943, and 2882 cm^{-1} in the spectrum of the classic-UiO-66 sample and 3068, 2964, 2904, and 2876 cm^{-1} characterize asymmetric and symmetric valence vibrations in $-CH_3$- and $-CH_2$-fragments of bdc-linkers. Several bands in the region 2000-1670 cm^{-1} belong to overtones of deformation vibrations of the δC-H bond (nonlinear and multiplet). The region 1670–1500 cm^{-1} (classic-UiO-66) and 1650–1550 cm^{-1} (PET-UiO-66) includes the bands corresponding to valence vibrations of the νC-C bond in the aromatic ring of the bdc-linkers. The bands at 1603 and 1454 cm^{-1} (classic-UiO-66) and 1596 and 1442 (PET-UiO-66) correspond to the νC = C-bond in the aromatic ring of the bdc-linkers (Fig. 5). The bands in the region 1300–1000 cm^{-1} in the spectra of both materials correspond to planar strain vibrations in the aromatic ring of the bdc-linkers.

Thus, the same functional groups are present on the surface of the PET-UiO-66 samples and the classic-UiO-66 reference sample, indicating the formation of the UiO-66 framework based on the secondary PET, the bdc-linker source. Some differences are observed in the composition of the μ_3-OH building blocks, which may be due to the presence of defects in the PET-UiO-66 structure. Such defects may be due to high concentrations of reagents used in the synthesis process.

Studying thermal stability of the PET-UiO-66 sample by the TGA method. The observed pattern of mass change of the PET-UiO-66 sample during its heating in the air atmosphere reflects its stepwise thermo-oxidative degradation. The total mass loss of the PET-UiO-66 sample is 57.2%: 0.8% up to ~140°C, 27.5% in the range 140–450°C, 24.7% at 450–590°C, and 4.0% at 590–675°C. For a more complete characterization of the PET-UiO-66 sample, the thermal stability of the classic-UiO-66 material synthesized according to the classical methodology [17] was also studied.

Comparing the TGA and DTA curves (Fig. 6) for UiO-66 materials synthesized on the basis of PET and according to the "classical" technique, we can see that for the PET-UiO-66 material the region of 200–420°C corresponds to the thermal degradation of residual PET oligomers. The first maximum of the thermal effect (540°C), as well as the respective region 420–600°C, are characteristic both for the PET-UiO-66 material and for the classic-UiO-66 sample and correspond to the destruction of the framework. The second maximum of thermal effect (640°C) and its respective region on the

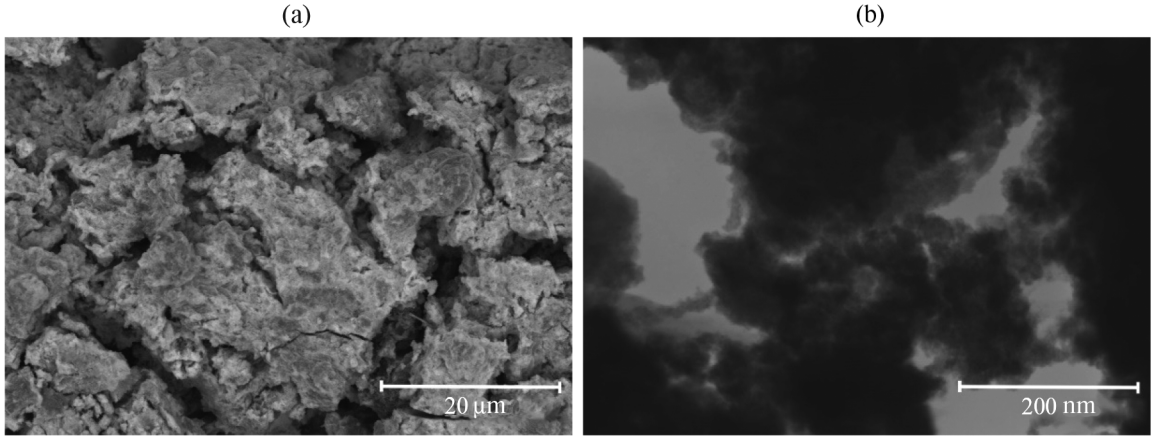

Fig. 3. SEM (a) and STEM (b) images of the PET-UiO-66 material.

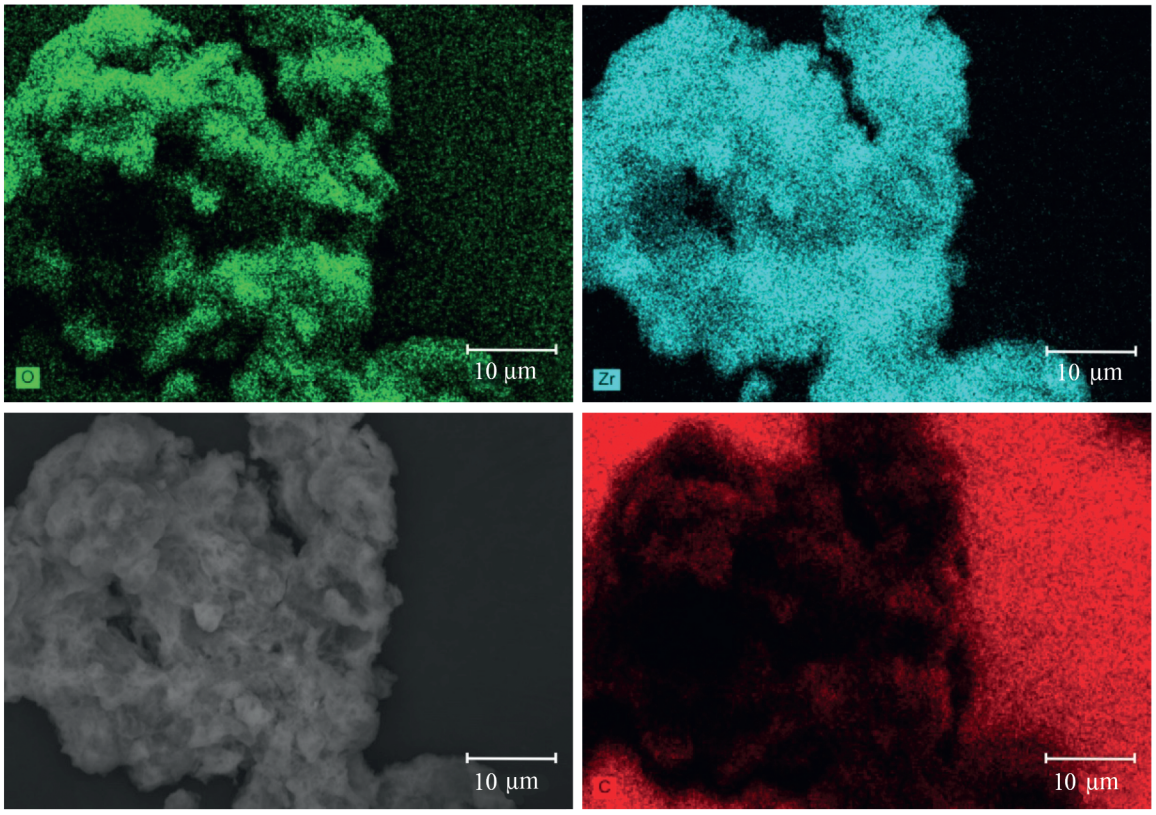

Fig. 4. SEM-EDX mapping of the PET-UiO-66 material.

TGA curve are characteristic only for the PET-UiO-66 material. They may correspond to the oxidation of carbon formed during thermal destruction of residual oligomers formed during PET depolymerization. Based on the weight change of the sample during thermal decomposition, it contains ~4.5% impurity of residual PET oligomers.

Thus, the characterization results for PET-UiO-66 material indicate that its physicochemical characteristics correspond, in the principal details, to the properties of UiO-66 samples known from publications.

Adsorption of tartrazine on the PET-UiO-66 material. To reveal the adsorption behavior of the PET-UiO-66 material towards tartrazine, kinetic and thermodynamic measurements were carried out in a wide concentration range (25–150 mg/L). The determination of adsorption kinetics reflects the mass transfer mechanism in this process as well as the rate of the limiting stage [39].

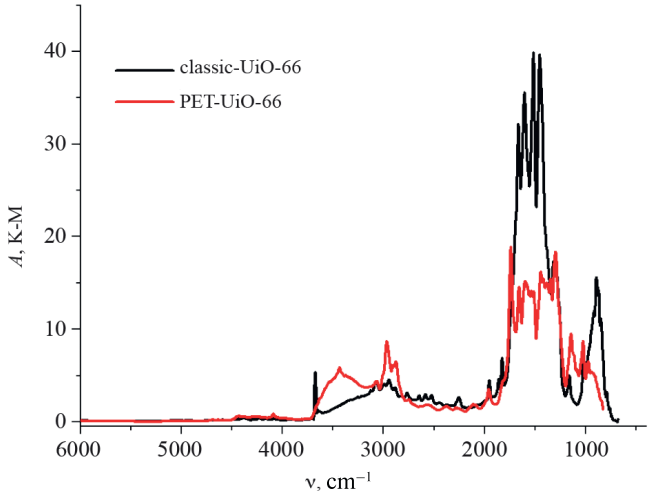

Fig. 5. Overview spectra of the classic-UiO-66 and PET-UiO-66 samples after thermal vacuum treatment (150°C).

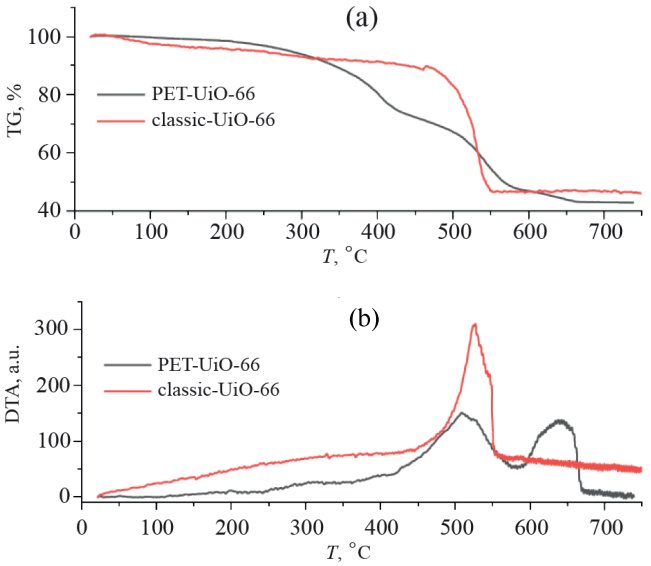

Fig. 6. TG (a) and DTA (b) curves for the PET-UiO-66 and classic-UiO-66 materials.

As shown in Fig. 7, adsorption equilibrium is reached in ~100 h. The pseudo-first order (PF) model [40], pseudo-second order (PS) model [41], and Elovich equation [42] were used to study the adsorption kinetics of tartrazine. The pseudo-first order model is expressed by the equation

$$q_t = q_e\left(1-\exp^{-k_1 t}\right), \quad (1)$$

where $k_1(\text{min}^{-1})$ is the rate constant, q_e and q_t (mg/g) are the amount of adsorbed adsorbate at equilibrium and in time, respectively.

The pseudo-second-order model equation is expressed as

$$q_t = \frac{q_e^2 \cdot k_2 \cdot t}{1 + q_e^2 \cdot k_2 \cdot t}, \quad (2)$$

where k_2 (l/(mg min)) is the adsorption rate constant of the PS model. The Elovich model is described by the equation [42]

$$q_t = \frac{1}{\beta} \cdot \ln(\alpha \cdot \beta \cdot t + 1), \quad (3)$$

where α (mg/(g min)) is the initial adsorption rate, and β (g/mg) is the desorption constant during each experiment.

Figure 7 shows the results of tartrazine adsorption experiments on the PET-UiO-PET sample and the adsorption curves corresponding to PF, PS, and Elovich model. The parameters calculated by the above models are given in Table 1. These data indicate that the PS model gives the best fit with higher regression coefficients (R^2 = 0.994–0.999). Thus, the process kinetics is consistent with the PS equation.

Three principal models — Langmuir [43], Freundlich [44], and Temkin [45], were used to describe the adsorption isotherms of tartrazine on the PET-UiO-66 sample. The nonlinear form of the Langmuir isotherm can be described as follows

$$q_e = q_m b_l c_e / (1 + b_L c_e), \quad (4)$$

where q_m is the maximum monolayer capacity (mg/g), and b_l is the adsorption coefficient (l/g).

Mathematically, the Freundlich isotherm can be represented as the equation

$$q_e = K_F c_e^{1/n}, \quad (5)$$

where K_F is the distribution coefficient or adsorption coefficient (l/g).

The Temkin model is described by equation (6) [45]

$$q_e = (RT / b_T) \cdot \ln(A c_e), \quad (6)$$

where b_T is the adsorption coefficient (J/mol), R is the universal gas constant 8.314 J/(mol K), A is a constant (l/g), and T is the absolute temperature (K).

Figure 8 shows the adsorption isotherms of tartrazine on the PET-UiO-66 sample for different models. Experimental and calculated parameters for each model isotherm are given in Table 2. Analysis of the data in Table 2 — a comparison of the values of the parameter R^2 — indicates that the Langmuir equation is more representative than the Temkin and Freundlich

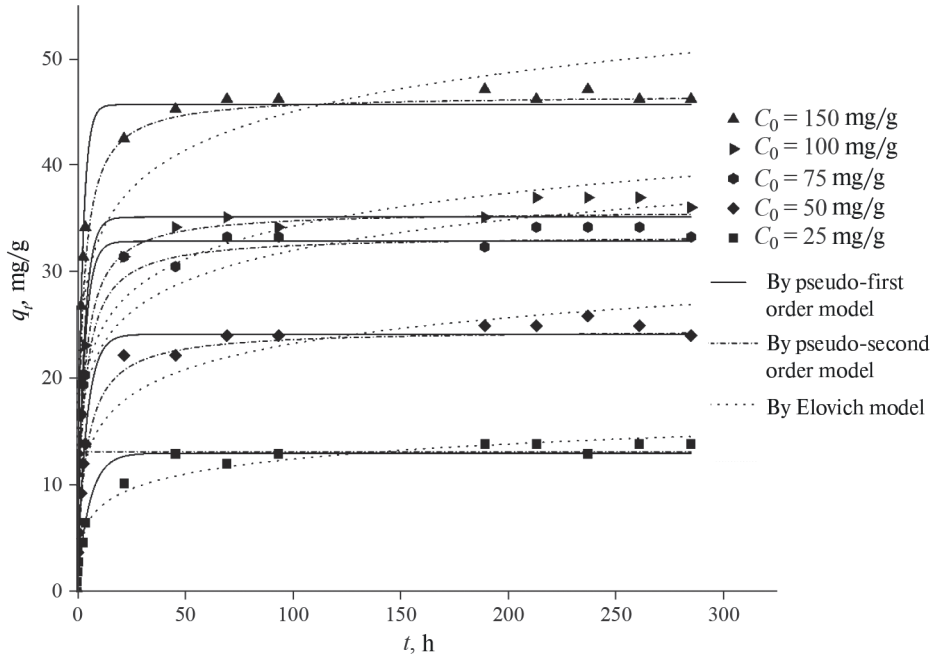

Fig. 7. Adsorption kinetics of tartrazine on the PET-UiO-66 sample. Dots stand for the experimental data, and lines stand for the model calculations.

Table 1. Parameters of the kinetic models of the tartrazine adsorption process on the PET-UiO-66 material

C_0, mg/l	Pseudo-first order			Pseudo-second order			Elovich equation			q_e exp, mg/g
	k_1	q_e , mg/g	R^2	k_2	q_e , mg/g	R^2	α, mg/(g min)	β, g/mg	R^2	
25	0.17	13.05	0.970	0.02	13.76	0.990	0.15	0.488	0.978	13.9
50	0.23	24.20	0.991	0.01	25.19	0.996	0.43	0.283	0.960	24.1
75	0.31	32.96	0.982	0.01	33.90	0.994	1.44	0.238	0.954	33.4
100	0.32	35.24	0.980	0.01	36.28	0.994	0.93	0.582	0.966	36.1
150	0.43	45.79	0.987	0.02	46.87	0.999	4.54	0.190	0.980	46.3

equations. Hence, the correspondence of the adsorption process of tartrazine on the PET-UiO-66 material to the Langmuir equation indicates that the surface of this adsorbent is basically homogeneous, monolayer adsorption of adsorbate on the adsorbent surface is realized, and there are no interactions between adsorbed particles [43].

CONCLUSIONS

In this work, the UiO-66 material using secondary polyethylene terephthalate as a source of an organic linker for framework construction was prepared by the original technique under microwave activation of reaction mass at atmospheric pressure without using acids and other agents promoting depolymerization. In this case, resource-saving high-performance (at high concentrations of reagents) synthesis of the PET-UiO-66 sample in the "green" non-conventional solvent triethylene glycol for a short time (30 min) is implemented.

The fact that the PET-UiO-66 sample corresponds to the "classical" UiO-66 structure was confirmed by physicochemical methods. The PET-UiO-66 material was studied in the process of adsorption of the tartrazine food dye, toxic at high concentrations, from aqueous solutions for the first time. The adsorption on the PET-UiO-66 sample is consistent with the pseudo-second-order kinetic model and the Langmuir thermodynamic model. Preparing the PET-UiO-66 adsorption material using recycled PET can contribute to solving the problems of recycling polymer waste into value-added products and removing persistent organic pollutants from water.

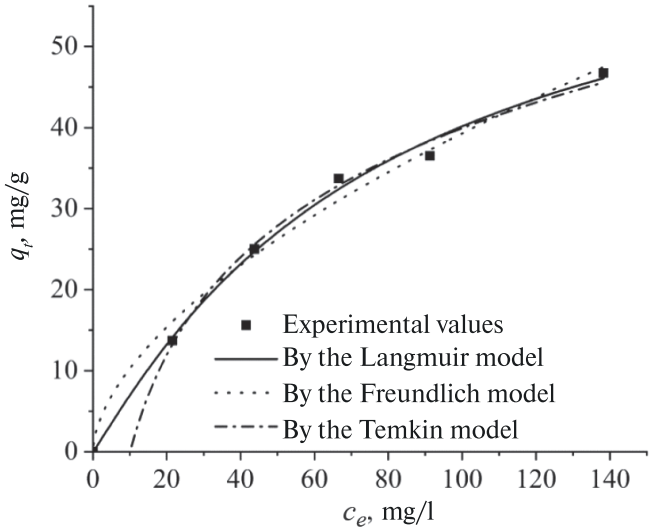

Fig. 8. Tartrazine adsorption isotherms on the PET-UiO-66 material.

Table 2. Parameters of tartrazine isotherms on the PET-UiO-66 sample

Model	Model parameters	Values
Langmuir	q_m, mg/g	78.04
	b_l, l/g	0.011
	R^2	0.998
Freundlich	K_F, mg/g	31.12
	$1/n$	4.34×10^{-11}
	R^2	0.762
Temkin	b_T, J/mol	504.0
	A, l/g	5.04
	R^2	0.936

CONFLICT OF INTEREST

The authors of this work declare that they have no conflicts of interest.

ACKNOWLEDGEMENTS

The authors would like to thank the Department of Structural Research of the Institute of Organic Chemistry of Russian Academy of Sciences for studying the samples by electron microscopy.

FUNDING

This work was supported by the Russian Science Foundation (grant no. 23-73-30007).

REFERENCES

1. *Chaturvedi P., Shukla P., Giri B.S. et al.* // Environmental Res. 2021. Vol. 194. P. 110664.
2. *Ezzatahmadi N., Marshall D.L., Hou K. et al.* // J. Environ. Chem. Eng. 2019. Vol. 7. P. 102955.
3. *Tang J., Wang T., Xia H. et al.* // Sustainability. 2024. Vol. 16. P. 2042.
4. *Ariza-Tarazona M.C., Siligardi C., Carrėon-Lŏpez H.A. et al.* // Marin. Pollut. Bull. 2023. Vol. 193. P. 115206.
5. *Yang R.X., Bieh Y.T., Chen C.H. et al.* // ACS Sustainable Chem. Eng. 2021. Vol. 9. P. 6541.
6. *Kartik S., Balsora H. K., Sharma M. et. al.* // Therm. Sci. Eng. Progr. 2022. Vol. 32. P. 101316.
7. *Ferreira M.M., Silva E.A., Cotting F. et. al.* // Corros. Eng. Sci. Technol. 2021. Vol. 56. P. 199.
8. *Kaur G., Uisan K., Ong K.L. et. al.* // Cur. Opin. in Green and Sust. Chem. 2018. Vol. 9. P. 30.
9. *Yang R.X., Bieh Y.T., Chen C. H. et. al.* // ACS Sustainable Chem. Eng. 2021. Vol. 9. P. 6541.
10. *Rowsell J.L., Yaghi O.M.* // Microporous and Mesoporous Mat. 2004. Vol. 73. P. 3.
11. *Ghazvini M.F., Vahedi M., Nobar S.N. et al.* // J. Environ. Chem. Eng. 2021. Vol. 9. P. 104790.
12. *Ihsanullah. I.* // Curr. Opin. Environ. Sci. Health. 2022. Vol. 26. P. 100335.
13. *Obeso J.L., Flores J.G., Flores C. V. et al.* // Chem. Commun. 2023. Vol. 59. P. 10226.
14. *Baumann A.E., Burns D.A., Liu B. et al.* // Commun Chem. 2019. Vol. 2. P. 86.
15. *Mendes R.F., Figueira F., Leite J. P. et al.* // Chem. Soc. Rev. 2020. Vol. 49. P. 9121.
16. *Isaeva V.I., Vedenyapina M.D., Kurmysheva A.Y. et. al.* // Molecules. 2021. Vol. 26. P. 6628.
17. *Cavka J., Jakobsen S., Olsbye U. et al.* // JASC Com. 2008. Vol. 140. P. 42.
18. *Kazemi A., Moghadaskhou F., Pordsari M.A. et al.* // Sci Rep. 2023. Vol. 13. No. 19891.
19. *Ahmadijokani F., Molavi H., Rezakazemi M. et al.* // Prog. Mater. Sci. 2022. Vol. 125. P. 100904.
20. *Rego R.M., Kurkuri M.D., Kigga, M.* // Chemosphere 2022. Vol. 302. P. 134845.
21. *Ramanayaka S., Vithanage M., Sarmah A. et al.* // RSC Adv. 2019. Vol. 9. P. 34359.
22. *Cao Z., Fu X., Li H. et al.* // ACS Sustain. Chem. Eng. 2023. Vol. 11. P. 15506.
23. *Shanmugam M., Chuaicham C., Augustin A. et al.* // New J. Chem. 2022. Vol. 46. P. 15776.
24. *Lo S.H., Raja D.S., Chen C.-W. et. al.* // Dalton Trans. 2016. Vol. 45. P. 9565.
25. *Dyosiba X., Ren J., Musyoka N.M. et al.* // Ind. Eng. Chem. Res. 2019. Vol. 58. P. 17010.

26. *Semyonov O., Kogolev D., Mamontov G. et al.* // Chem. Eng. J. 2022. Vol. 431. P. 133450.
27. *Selahle S.K., Nqombolo A., Nomngongo P.N.* // Sci Rep. 2023. Vol. 13. P. 6808.
28. *Waribam P., Katugampalage T.R., Opaprakasit P. et. al.* // Chem. Eng. J. 2023. Vol. 473. P. 145349.
29. *Oymak T., Tokalıoglu S., Cam S. et al.* // Food Additiv. Contamin. 2020. Vol. 37. P. 731.
30. *Singh H., Goyal A., Bhardwaj S. et al.* // Mater. Sci. Eng. 2023. Vol. 288. P. 116165.
31. *Kachala V.V., Khemchyan L.L., Kashin A.S. et al.* // Chem. Usp. 2013. Vol. 82. P. 648.
32. *Kashin A.S., Ananikov V.P.* // Russ. Chem. Bull. 2011. Vol. 60. No. 12. P. 2602.
33. *Tsyganenko A.A., Filimonv V.N.* // J. Mol. Struct. 1972. Vol. 5. P. 477.
34. *Ivanov A.V., Kustov L.M.* // Russ. Chem. Bull. 2000. Vol. 49. P. 39.
35. *Köck E.M., Kogler M., Götsch T. et. al.* // Dalton Trans. 2017. Vol. 46. P. 4554.
36. *Jung K.D., Bell A.* // J. Catal. 2000. Vol. 193. P. 207.
37. *Ouyang F., Kondo J.N.* // JCS Faraday Trans. 1996. Vol. 92. P. 4491.
38. *Cheng X., Zhang A., Hou K. et. al.* // Dalton Trans. 2013. Vol. 42. P. 13698.
39. *Huang J., Yan Z.* // Langmuir. 2018. Vol. 34. P. 1890.
40. *Lagergren S.* // Sakademiens Handl. 1898. Vol. 24. P. 1.
41. *Ho Y.S., Mckay G.* // Proc. Biochem. 1999. Vol. 34. P. 451.
42. *Zeldowitsch J.* // Acta Physicochim. 1934. Vol. 1. P. 364.
43. *Langmuir I.* // Part I. Solids. 1916. Vol. 184. P. 102.
44. *Dippong T., Andrea E., Cadar O. et. al.* // J. of Alloys and Comp. 2020. Vol. 849. P. 156695.
45. *Srivastava V., Sharma Y.C., Sillanpää M.* // Applied Surf. Sci. 2015. Vol. 338. P. 42.